Environmental Pollution 363 (2024) 125193

Contents lists available at ScienceDirect

Environmental Pollution

journal homepage: www.elsevier.com/locate/envpol

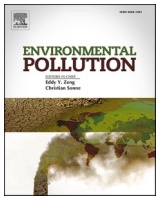

Effect of particle size on the transport of polystyrene micro- and nanoplastic particles through quartz sand under unsaturated conditions☆

Cynthia Rieckhof [a,b,*], Virtudes Martínez-Hernández [b], Ekkehard Holzbecher [c], Raffaella Meffe [b]

[a] University of Alcalá, Geology, Geography and Environment Science Department, 28802 Alcalá de Henares, Spain
[b] IMDEA Water Institute, Avda. Punto Com 2, 28805 Alcalá de Henares, Spain
[c] GUtech, PO Box 1816, Athaibah PC 130, Muscat, Sultanate of Oman

ARTICLE INFO

Keywords:
Nanoplastics
Microplastics
Column experiments
Numerical transport modelling
Particle size
Porous media
Unsaturated conditions

ABSTRACT

Micro- and nanoplastics (MNPs) are contaminants of emerging concern recently found in soil ecosystems. Their presence in terrestrial environments and their migration to aquatic environments may become a risk for the health of ecosystems and, through them, of humans. Understanding the interaction between particle properties and physicochemical and hydrodynamic factors is crucial to evaluate their fate and their potential infiltration towards groundwater. This study investigates the impact of particle size on MNPs transport through sand under unsaturated conditions. Infiltration column experiments with polystyrene MNPs ranging from 120 to 10,000 nm were conducted and supported by numerical modelling to derive reactive transport parameters. Results show a significant effect of particle size on the transport of MNPs, with higher recovery values observed for smaller particles (120 nm; 95.11%) compared to larger particles (1000 nm; 71.44%). No breakthrough was observed for 10,000 nm particles, indicating a complete retention within the quartz sand matrix. DLVO theory confirmed the dominance of electrostatic repulsive forces between MNPs and sand grains, suggesting an unfavourable environment for MNPs to adhere to quartz sand. Consequently, particle retention in the sand matrix occurs predominantly by physical processes. Equilibrium sorption modelling reveals that larger particles (1000 nm) tend to be immobilized in small pores throats due to straining, resulting in lower recoveries. When they are not trapped, particles tend to travel faster through preferential flows due to a size exclusion effect, evidenced by shorter arrival times at the column outlet compared to tracers. These findings highlight the influence of particle size on the transport and retention of MNPs in quartz sand under unsaturated conditions and contribute to a better understanding of their transport dynamics and environmental fate.

1. Introduction

In recent years, the inadequate production and management of plastic materials have led to the uncontrolled release of plastic waste into marine and terrestrial ecosystems, and it is becoming a widespread environmental concern (Hurley and Nizzetto, 2018). The breakdown of larger plastics, commonly used in agricultural activities, into micro- (<5 mm) and nanoplastics (<1 μm) by fragmentation and degradation processes (Hidalgo-Ruz et al., 2012) contributes to an uncontrolled accumulation of these contaminants in natural soils. A recent study estimates that the global average stock of microplastics in agricultural soils is about 3.6 Mt (Kedzierski et al., 2023). Once in the soil, small-sized micro- and nanoplastics (MNPs) can infiltrate through the vadose zone, potentially reaching groundwater. Additionally, these MNPs can increase the risk of contaminating aquifers due to the spread of other hazardous pollutants by colloid-facilitated transport (Zhou et al., 2022). Therefore, groundwater contamination by MNPs could pose a threat to the availability of drinking water, especially in regions where groundwater is the main source of water supply (Rajan et al., 2024). Literature reports that ingestion has been identified as one of the main routes of entry of MNPs into the human body, as MNPs of various sizes have been detected in human tissues and fluids, including the lungs, blood, colon, saliva, and urine (Kutralam-Muniasamy et al., 2023). Consequently, human exposure to these contaminants has been associated with adverse

☆ This paper has been recommended for acceptance by Eddy Y. Zeng.

* Corresponding author. University of Alcalá, Department of Analytical Chemistry, Physical Chemistry and Chemical Engineering, 28871, Alcalá de Henares, Madrid, Spain.
E-mail address: cynthia.rieckhof@edu.uah.es (C. Rieckhof).

https://doi.org/10.1016/j.envpol.2024.125193
Received 26 July 2024; Received in revised form 7 October 2024; Accepted 23 October 2024
Available online 24 October 2024

effects such as endocrine disorders and cardiovascular diseases (Winiarska et al., 2024). Therefore, the consumption of water contaminated with MNPs could also pose a threat to the human health. This potential toxicological risk to human health underlines the need to investigate the transport pathways of MNPs through soils as an entry route to groundwater.

The movement of MNPs is influenced by their inherent properties, including polymer type (Gao et al., 2021), particle size (Wang et al., 2022), shape (Keller et al., 2020), and functional group (Song et al., 2019). Moreover, aging processes lead to alterations of MNPs properties, including adsorption capacity, stability, and functional groups (Xi et al., 2022). In this sense, Yasir et al. (2022) recognize that the carboxyl functional group (COOH) is the most predominant on the surface of MNPs after the exposure to these processes and its occurrence affect particle behavior, toxicity and fate (Zhang et al., 2022). At the same time, environmental factors like the porous medium, soil pH, ionic strength, water chemistry (Wu et al., 2022), and soil water content (Dong et al., 2022) are crucial for MNPs displacement.

Different mechanisms have been proposed to describe the retention of contaminants during their transport through the vadose zone, including surface deposition, straining, and attachment at the solid-water (SWI) and air-water interface (AWI) (Bradford and Torkzaban, 2015; Dong et al., 2022). Straining, for instance, involves colloid entrapment in small-sized pores and becomes more significant with low moisture content (Zhang et al., 2021), low interstitial velocities, and small pore spaces (Yu and Flury, 2021). On the other hand, the DLVO theory (Derjaguin and Landau, 1993; Verwey, 1947) has been extensively used to elucidate the mechanism of colloid adhesion based on the total interaction energy between colloids and grain surface. Factors such as particle size, surface charge, and ionic strength can significantly influence the development of an energy barrier between colloids and sand, thereby preventing colloidal retention on the sand surface (Hotze et al., 2010). In addition to these factors, under unsaturated conditions, colloids can interact with the hydrophobic forces present at the AWI. The dominance of the van der Waals or the electrostatic forces can promote or hinder colloid retention in the AWI. Furthermore, if the colloids penetrate the AWI, capillary forces can keep particles attached to the interface (Aramrak et al., 2014). This theoretical framework has also been applied in prior studies to examine the aggregation of nanoplastic particles (NPs) with sand under both saturated (Wang et al., 2022) and unsaturated conditions (Dong et al., 2022).

Numerous authors have developed numerical models to elucidate the mechanisms underlying colloidal mobility (Flury and Qiu, 2008; Jin et al., 1997; Sim and Chrysikopoulos, 1995). Some studies on MNPs employ models based on the advection-dispersion equation to simulate the migration of these contaminants through soil matrices and to estimate transport parameters. Two types of modelling approaches are predominantly used to describe the MNP transport in soils: one-site kinetic retention model which assumes the irreversible retention of MNPs, and a two-site kinetic retention model that describes the attachment and detachment of MNPs onto/from the porous material (Xi et al., 2022; Yasir et al., 2022). Lin et al. (2021) also consider processes such as surface deposition and hydrodynamic bridging to take into account those mechanisms that control colloid retention. These approaches enable the prediction and understanding of the effects of hydrodynamic and physico-chemical properties (such as particle size, surface functionalization, grain size, flow rate) on the transport dynamics of MNPs (Li et al., 2024; Shaniv et al., 2021; Zhao et al., 2023). The ability to simulate and predict these intricate processes not only enhances the fundamental understanding of colloidal mobility but also holds significant implications for environmental dynamics. Thus, it provides a tool for assessing the potential risk of aquifer contamination and human exposure through drinking water.

The combination of MNP properties with environmental factors, such as the water content, could influence their vertical migration through soil. However, to our knowledge, studies simultaneously evaluating the combined effect of particle size and unsaturated conditions using modelling approaches are not available in the literature. A recent work by Wang et al. (2022) assessed the effects of particle sizes on the transport of MNPs through water-saturated quartz sand columns. Whereas an earlier study by Mitropoulou et al. (2013) analyzed the transport of MNPs with different sizes under unsaturated conditions. Although meaningful results were obtained, modelling tools able to quantify transport parameters were not applied. For this reason, studies that specifically evaluate the combined effect of both factors while minimizing experimental artifacts and quantifying transport parameters to help in predicting MNP fate under different scenarios are of pivotal importance. The authors believe that research in this area is pivotal for developing effective strategies to manage MNP pollution in terrestrial environments and its potential transfer to groundwater, since infiltration dynamics primarily occur under unsaturated conditions. In this context, this study aims to improve the understanding of those factors influencing MNP vertical transport under unsaturated conditions, evaluating and predicting the risk of subsurface contamination using controlled column experiments. Polystyrene MNPs of various sizes (120 - 10,000 nm) were used to assess the influence of particle size on their transport through quartz sand. Additionally, numerical modelling techniques were employed to quantify the transport parameters of MNPs in the porous media.

2. Materials and methods

2.1. Micronanoplastics and porous media

Fluorescent polystyrene MNPs with a particle size of 120, 500 and 1000 nm were purchased from Ikerlat Polymers (Gipuzkoa, Spain) whereas 10,000 nm particles were purchased from Bangs Laboratories, Inc (Fishers, USA). Selected MNPs were spherical particles, with a density of 1.054 g cm^{-3} and with carboxyl functional groups (COOH) (Table S1).

The MNP suspensions (20 g L^{-1}) were sonicated for a homogeneous distribution of the particles and then diluted with tap water to achieve a target input concentration of 40.95 ± 1.43 mg L^{-1}. Input concentration was selected based on the detection limits of the available analytical method (described in the next section). The suspensions were stored in the dark at 4 °C.

Commercial quartz sand with a mean particle size ranging from 0.5 to 0.8 mm was selected as target porous media. Prior to the experiments, the sand was soaked in 30% nitric acid (HNO_3) for 24 h and washed with deionized water. Successively, it was soaked in 2 mmol L^{-1} NaOH for 24 h and washed repeatedly with deionized water to remove metal oxides and organic impurities. The purified quartz sand was dried at 40°C during 24 h.

2.2. Column transport experiments

MNP transport experiments were run per triplicate using an *ad hoc* designed plastic-free system (Fig. S1 in Appendix A) with glass columns (L: 20 cm and ID: 5 cm). A glass porous plate with a thickness of 1 cm and a mean pore size between 250 and 500 μm was placed at the bottom of each column to prevent loss of the porous matrix. A 2 cm layer of glass fragments (size: 1–5 mm) (NatureWorks, Alicante, Spain) were placed right above the porous plate to prevent its clogging. To ensure homogeneous packing, columns were gradually filled with sand increments of 1 cm until reaching a total thickness of 10 cm and a bulk density of 1.75 g cm^{-1}. At the upper end of each column, a glass fragments layer of 1 cm was placed to ensure a uniform distribution of the influent. On the other hand, each effluent was collected in a closed deposit to prevent external contamination.

Columns were previously saturated with tap water by an upward flow to avoid the entrapment of air bubbles using a peristaltic pump (Masterflex® L/S® 07528-20/30). After saturation, the total porosity of

the sand (0.36 ± 0.02) was obtained gravimetrically. Columns were allowed to drain by gravity. Subsequently, the water flow was inverted, and a downward flow was established simultaneously to the application of a negative pressure (suction) at the bottom of the column. Suction pressure was increased gradually until obtaining a constant water flow that matched the inlet flow (0.5 mL min^{-1}). Such a set-up guaranteed unsaturated conditions throughout the entire sand profile and a homogeneous distribution of the water content. The sand saturation degree during the experiments was 48.5 ± 1.5%, corresponding to a water content of 34.4 ± 1.9 mL.

Each experiment began with the injection of 7 pore volumes (PVs) of tap water to achieve chemical and hydrodynamic stabilization of the system. Successively, 4 PVs of MNP solution were injected at the inlet of each column using a flow rate of 0.51 ± 0.02 mL min^{-1}. This phase was followed by a flush out step introducing 6 PVs of tap water (free of targeted MNPs) at the same flow rate. Finally, to obtain sand hydraulic transport parameters, a tracer test was performed under the same experimental conditions of the MNP transport test using potassium chloride (KCl) salt. To this end, 3 PVs of a KCl solution with a concentration of 5 g L^{-1} were injected into each column and successively flushed by 4 PVs of tap water. All effluent samples were collected every 30 min and stored in amber bottles at 4°C.

The concentration of MNPs at the column effluents was determined using a UV-1800 UV–VIS spectrophotometer (Shimadzu, Japan) at wavelengths of 576 nm for 120 and 500 nm, 427 nm for 1000 nm and 501 nm for 10,000 nm MNPs. Linear calibration curves were used to calculate the concentration of the MNPs in the samples. Calibration curves were performed by spiking MNPs in the effluent prior to the injection of MNPs to consider potential matrix interferences in the quantification. Method detection limit (MDL) and method quantification limit (MQL) are 0.72 and 2.41 mg L^{-1} for 120 nm, 0.36 and 1.19 mg L^{-1} for 500 nm, 0.50 and 1.67 mg L^{-1} for 1000 nm and 2.47 and 7.14 mg L^{-1} for 10,000 nm, respectively. Values bellow the MDL are considered as zero for calculations.

The determination of the tracer breakthrough curve was obtained by measuring the electrical conductivity (EC) of the samples with a multimeter (Crison, Spain). The EC values were transformed to total dissolved solids (TDS) by applying the following formula (1):

$$\mathrm{TDS}\ (\mathrm{mg\ L^{-1}}) = (\mathrm{EC\text{-}EC_0})\mathrm{CF} \quad (1)$$

Where EC_o is the background EC (μS cm^{-1}) measured before tracer injection and CF (−) is the conversion factor allowing for total mass recovery of the tracer (Lloyd and Heathcote, 1985). However, Cl^- concentrations were also periodically measured to confirm the reliability of using TDS.

Z-average hydrodynamic particle size (D) and zeta potential (ϕ) of both, the quartz sand and NP particles, were measured in influent and effluent samples with the highest NP concentration (plateau region of the breakthrough curves), using a Zetasizer Nano ZS (Malvern Panalytical, UK). The zeta potential is a parameter that characterizes the particle's surface charge and serves as an indicator of the colloidal suspension stability (Dong et al., 2018).

To minimize plastic contamination, the glass material (e.g. column, tubes, vials) used in the experiments was washed with 70% ethanol and MilliQ water prior to its use. The injected MNP solution was continuously stirred to avoid particle aggregation.

2.3. DLVO

The DLVO theory (Derjaguin and Landau, 1993; Verwey, 1947) was used to calculate the interaction energy (V_{TOT}) (2) between NP-NP, NP-sand and NP-AWI. However, since the DLVO theory is typically applied to colloidal systems, it may not be applicable to 10,000 nm MP, as they exceed the established size range of colloidal particles.

The total interaction energy is described as the sum of the attractive van der Waals interaction V_{VDW} (3, 4) and the repulsive electrostatic double layer interaction V_{EDL} (5, 6).

$$V_{TOT} = V_{VDW} + V_{EDL} \quad (2)$$

The attractive van der Waals interaction (Gregory, 1981) is calculated by (3) for NP-NP interaction and (4) for NP-Sand and NP-AWI interaction.

$$V_{VDW} = -\frac{A_{131}\ r_{NP}}{6h\left(1+\frac{14h}{\lambda}\right)} \quad (3)$$

$$V_{VDW} = -\frac{A_{132}\ r_{NP}}{6h\left(1+\frac{14h}{\lambda}\right)} \quad (4)$$

Where A_{131} represents the Hamaker constant for NP-NP [-4,2 x 10^{-21} J (Israelachvili, 1992)], A_{132} represents the Hamaker constant for NP-Water-Sand and NP-Water-Air [6,73 x 10^{-21} J and −1,2 x 10^{-20} J (Israelachvili, 1992)], respectively], r_{NP} is the NP radius (m), h is the separation distance between NPs, NPs and sand surface or AWI (m) and λ is the characteristic wavelength of interaction (10^{-7} m) (Elimelech et al., 1995).

The repulsive electrostatic double layer interaction (Gregory, 1975) is calculated by (5) for NP-NP interaction and (6) for NP-Sand and NP-AWI interaction.

$$V_{EDL} = 2\pi r_{NP}\varepsilon_0\varepsilon_r\phi_p^2\ \ln[1+\exp(\text{-}kh)] \quad (5)$$

$$V_{EDL} = \pi r_{NP}\varepsilon_0\varepsilon_r\left\{2\phi_p\phi_c\ \ln\left[\frac{1+\exp(\text{-}kh)}{1\text{-}\exp(\text{-}kh)}\right] + \left(\phi_p^2+\phi_c^2\right)\ln\left[1\text{-}\exp(\text{-}2kh)\right\}\right. \quad (6)$$

Where $\mathcal{E}_0$ is the vacuum permittivity (8.854 x 10^{-12} C V^{-1} m^{-1}), $\mathcal{E}_r$ is the relative dielectric permittivity of water (78,5), ϕ_p is the zeta potential of NP (Table S2) and ϕ_c is the zeta potential of the sand and AWI [-33.0 ± 3.5 mV and −46,5 mV (Dong et al., 2022), respectively]; and k is the Debye-Hückel parameter, defined by (7)

$$k = \sqrt{\frac{2N_A e^2 I}{\varepsilon_0\varepsilon_r K_B T}} \quad (7)$$

where N_A is Avogadro's number ($6.02{\cdot}10^{23}$ mol^{-1}), e is the electron charge (−1.60 x 10^{-19} C), I is the ionic strength of the background electrolyte solution (Table S2), K_B is Boltzmann constant (1.38 x 10^{-23} J K^{-1}), and T is temperature (298 K).

2.4. Modelling

The COMSOL Multiphysics software (COMSOL, 2019) was used to simulate the experimental breakthrough curves and estimate the transport parameters of MNP particles. A 1-D transport model was applied to describe the plastic migration within the porous media. This model includes advective and diffusive processes, de- and remobilisation, as well as deactivation. The diffusive processes are defined by an effective diffusivity that includes the longitudinal dispersivity. For advective transport, the mean pore water velocity was obtained by fitting tracer breakthrough curves, assuming a homogeneous distribution of water within the matrix. Concerning the plastic particle transport, an initial approach based on the equation developed by Chrysikopoulos and Syngouna (2014) was applied to evaluate the impact of gravity on MNP movement. However, this model underestimated the observed MNP velocities and was subsequently discarded. An equilibrium sorption model using a partition coefficient K_d that assumes an equilibrium between the free particles in the water and those attached onto the surfaces of the porous matrix was defined. Additionally, a linear loss term representing a permanent immobilisation of plastic particles in the columns

was included.

2.4.1. Equilibrium sorption model

The transport simulation for the equilibrium activation and deactivation based on the advection-dispersion equation is described by the following equation (8):

$$R\frac{\partial c}{\partial t}=\frac{\partial}{\partial x}D\frac{\partial c}{\partial x}-v\frac{\partial c}{\partial x}-\lambda c \quad (8)$$

Where c is the MNP concentration (M $L^{3\text{-}1}$), R is the retardation factor (−), D is the effective diffusivity (L^2 T^{-1}), v is the mean pore water velocity (L T^{-1}) and λ is the removal rate (T^{-1}). The latter represents permanent deactivation of MNP from transport, i.e. particles that are trapped in regions of small porosity or in dead-end pores, from which they are not released during the time of the experiment. Retardation results from temporary deactivation of MNP particles from transport in the fluid, being attached at the surfaces of the grains, from where they are finally released. For these processes of activation and deactivation the K_d approach, commonly used for sorption of chemical species, is used. In the case of linear sorption, the retardation factor (9) can be expressed as:

$$R=1+\frac{\rho_b K_d}{\theta} \quad (9)$$

where ρ_b denotes the bulk density (M L^{-3}), K_d the partition coefficient (L^3 M^{-1}) and ϑ the volumetric moisture content (−), the product of porosity and saturation. For the simulation of the conservative tracer, the approach given in equation (8) was also used with $\lambda = 0$. R then represents a correction factor for the real flow velocity and no real retardation.

The models simulate tracer and NP transport through the sand, applying a zero-concentration initial condition. At the inlet, a Dirichlet boundary condition with a given input concentration during the time of injection was introduced. At the outlet, the typical Neumann condition was considered. Since the 3-size nanoparticle transport experiments were accompanied by a tracer experiment, a total of 18 model runs were performed.

With all models, an extensive parameter estimation study was carried out. This included the parameters of effective diffusivity, partition coefficient and input concentration. The latter was allowed to change only within a small range representing the measurement error. The removal rate was included in the parameter list when simulating MNP particle transport. All runs were performed three times, using different optimization methods: Levenberg-Marquardt, SNOPT and BOBYQA (COMSOL, 2019). Moreover, parameter starting points, scales and bounds were varied to obtain the parameter combination with the least value of the objective function.

Table 1 summarizes the model input parameter of the replica for which the best data fit – the one with the smallest objective function – was obtained. The complete dataset for each particle size including all the replicas is available in Table S2.

3. Results and discussion

3.1. Hydrodynamic conditions in the quartz sand

Tracer experimental and simulated breakthrough curves are shown in Fig. S2. Under steady-state water flow conditions, the breakthrough curves of KCl show a typical shape, with a sharp initial curve and a gradual drop in the tailing part, consistent with tracer curves usually observed for homogeneous sand columns under unsaturated conditions (De Smedt and Wierenga, 1984; Huang et al., 1995; Nutzmann et al., 2002). The similarity between replicas of each experiment serves as an indicator of the reliability of the data acquired. As discussed in the next section, 10,000 nm MP were retained in the sand and modelling of both tracer and MP data were not performed. However, the experimental breakthrough curve of the tracer (Fig. S2D) reveals hydrodynamic conditions similar to those observed for the other experimental sets.

Table 1
Model input parameters of the best fit replica for each experiment.

Parameter		NP		
		120 nm	500 nm	1000 nm
Model domain	Profile length (cm)	10		
	No. of materials	1		
	No. of nodes	101		
Time domain	Output time step (min)	6.65		
	Simulation time (min)	665		
Hydraulic properties	Bulk density (g cm^{-3})	1.75		
	Flux (mL min^{-1})	0.50	0.50	0.53
	Porosity (−)	0.37	0.35	0.38
	Saturation (%)	46.88	52.55	50.27
Initial conditions	KCl (g L^{-1})	0		
	NP (mg L^{-1})	0		
Boundary conditions	Dirichlet at inlet			
	Neumann at outlet			
Parameter estimation from conservative transport	Effective diffusivity (m^2 s^{-1})			
	Partition coefficient (m^3 g^{-1})			
	Inflow concentration (g L^{-1})			
Parameter estimation from NP reactive transport	Effective diffusivity (m^2 s^{-1})			
	Partition coefficient (m^3 g^{-1})			
	Removal rate (s^{-1})			
	Inflow concentration (mg L^{-1})			
Parameter estimation methods	Levenberg-Marquardt			
	SNOPT			
	BOBYA			

The simulated breakthrough curves were calibrated by parameter estimation, as described in Table 1. The resulting values for effective diffusivity (D) and partition coefficient (K_d) are presented in Table 2.

3.2. Experimental breakthrough curves of MNPs

Breakthrough curves of 120, 500, 1000 and 10,000 nm MNPs through the quartz sand are represented in Fig. 1. As can be easily recognized by observing the plotted data, the curves of 120, 500 and 1000 nm NPs exhibit a similar shape, equivalent to the shape of the breakthrough curves of the tracer. The first nanoparticles reach the column outlet approximately 30 min after injection and their concentration reach the plateau region after approximately 120 min. As already described for tracer data, the similarity among replicas indicates data reliability. Conversely the larger particles (10,000 nm) are fully retained in the quartz sand.

The mobility of those particles able to spread towards the column outlet is significantly influenced by their particle size. In this sense, the lower the particle size the higher the maximum concentrations in the effluent, although none of the MNPs reach their initial concentration values. Specifically, 120 nm NPs achieve a peak concentration of 0.97 ± 0.01 (C/C_0), whereas this value decreases to 0.85 ± 0.03 for 500 nm NPs, to 0.77 ± 0.03 for 1000 nm NPs and to values below the MDL for

Table 2
Calibrated parameters from conservative transport simulation (effective diffusivity and partition coefficient), quality of the fit (objective function) and optimization method for the equilibrium sorption model.

Tracer Experiment	D (m^2 s^{-1})	K_d (m^3 kg^{-1})	Objective function	Method
120 nm	2.60E-8	3.30E-5	4.42E4	BOBYQA
500 nm	5.17E-8	2.58E-5	10.28E4	BOBYQA
1000 nm	5.77E-8	3.22E-5	7.08E4	LM

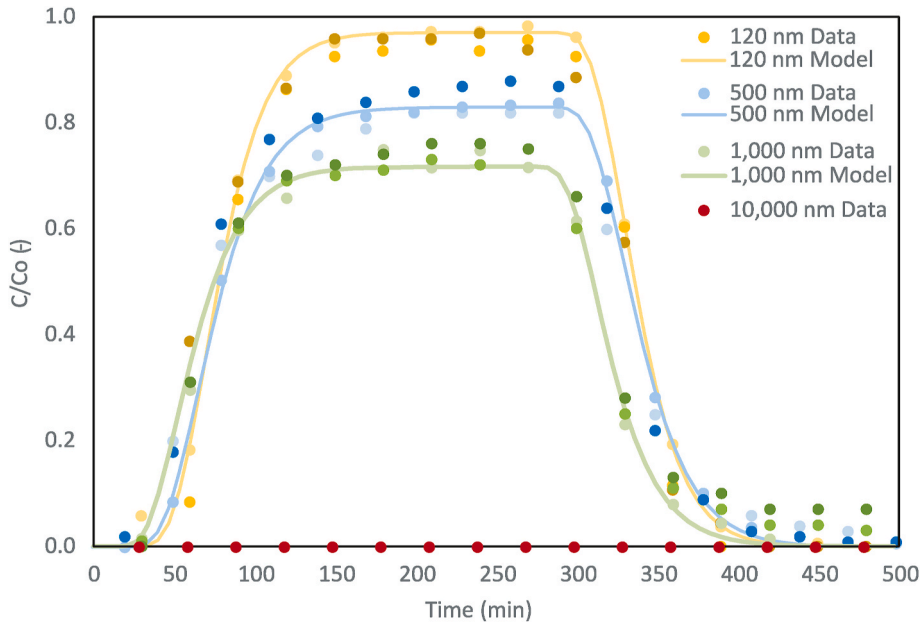

Fig. 1. Experimental breakthrough curves from 120, 500 and 1000 nm NPs. No breakthrough was obtained for 10,000 nm MNPs. Simulated breakthrough curve in each graph represents the best fit for each size.

10,000 nm MP. These findings suggest that smaller particles attained higher concentrations in the effluent when compared to larger particles. A similar behaviour was also observed in previous studies under saturated conditions (Bradford et al., 2002; Song et al., 2019; Wang et al., 2022).

MNP recovered masses provided in Table 3 were calculated taking into account effluent MNP concentration and drained volumes. In accordance with the maximum MNP concentration values observed in Fig. 1, particle mass recovery decreases with increasing particle size, exhibiting average values of 95.11 ± 2.93% for 120 nm, 85.73 ± 2.07% for 500 nm, 71.44 ± 3.30 % for 1000 nm, and values below the MDL for 10,000 nm MP. Under the experimental conditions and within tested NP size range (120-1000 nm), a linear correlation between mass recovery and particle size was observed (Fig. S3). This implies that the retention of particles in the sand is predominantly governed by physical processes. Applying the regression line equation, the particle size calculated for a 0% recovery is 3630 nm. Consequently, larger particles are expected to be completely retained in the sand column, as observed for the 10,000 nm MP used in this study. However, beyond the investigated size range (120-1000 nm), the confirmation of linearity becomes uncertain, as the transport of nanoparticles may vary based on their intrinsic properties. This is particularly pertinent for smaller particles (<50 nm), as they are more prone to homoaggregate due to their high relative surface energy (He et al., 2008; Hou et al., 2022). This likely results in an increased retention in porous media, impacting the overall particle transport behaviour.

Table 3
MNP input mass, maximum effluent concentration and mass recovery of the 3 replicas of each experiment. In bold, the replica for which a best modelling fit is obtained.

MNP	Replica	Injected mass (mg)	Recovered mass (mg)	Removed mass (mg)	Normalized maximum concentration (C/C_0) (−)
120 nm	**A**	**5.17**	**5.03 (97.19%)**	**0.14 (2.81%)**	**0.98**
	B	5.29	4.86 (91.76%)	0.43 (8.24%)	0.96
	C	5.02	4.84 (96.37%)	0.18 (3.63%)	0.97
500 nm	A	5.50	4.66 (84.87%)	0.84 (15.13%)	0.82
	B	**5.87**	**4.94 (84.23%)**	**0.93 (15.77%)**	**0.84**
	C	5.85	5.15 (88.09%)	0.70 (11.91%)	0.88
1000 nm	**A**	**5.68**	**4.10 (72.23%)**	**1.58 (27.77%)**	**0.80**
	B	5.64	4.19 (74.28%)	1.45 (25.72%)	0.75
	C	5.64	3.82 (67.82%)	1.82 (32.18%)	0.76
10,000 nm[a]	A	5.12	0	0	0
	B	5.01	0	0	0
	C	5.01	0	0	0

[a] All the measurements were below MDL.

3.3. Equilibrium sorption model for NP

Simulated breakthrough curves for 120, 500 and 1000 nm NPs obtained by the equilibrium sorption model are presented in Fig. 1. The model shows an excellent fit of the experimental data. Differences of the plateau values reflect the impacts of particle size on NP transport in porous media. Table 4 provides the corresponding reactive transport parameter values of the best fit (smallest objective function) among replicas. Retardation factor R is calculated from the K_d's according to equation (7). Note that for $R < 1$ the factor represents the opposite of retardation, i.e. increased advective transport. Fig. 2 lists the values of D, K_d and λ as functions of particle size and their variation among replicas.

Table 4
Best fit values from reactive transport parameters (effective diffusivity, partition coefficient, retardation factor, and removal rate), quality of the fit and optimization method for the equilibrium sorption model.

NP	D (m^2 s^{-1})	K_d (m^3 kg^{-1})	R (−)	λ (s^{-1})	Objective function	Optimization Method
120 nm	3.59E-8	2.50E-5	1.00	1.87E-6	3.36	LM
500 nm	4.88E-8	1.77E-5	0.94	6.77E-6	2.21	LM
1000 nm	6.78E-8	0.75E-5	0.82	17.0E-6	5.63	BOBYQA

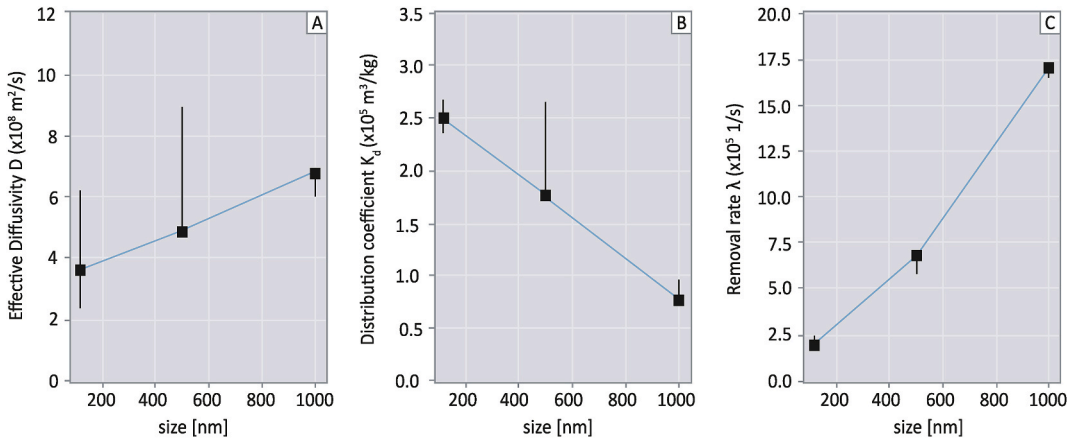

Fig. 2. Values of (A) effective diffusivity, (B) partition coefficient and (C) removal rate as a function of particle size. The black bars show variations of the parameter obtained from the values of the replicas. The blue line connects the values for which the best fit was obtained. (For interpretation of the references to colour in this figure legend, the reader is referred to the Web version of this article.)

The results show a decrease of K_d values with increasing particle sizes (Fig. 2B), indicating increased advective transport. Such a behaviour can be attributed to size exclusion effect. This process has been evoked by several authors to describe a colloid-facilitated transport of groundwater contaminants (Babakhani, 2019; Bradford et al., 2003; You et al., 2013). Due to their size, larger particles that are more likely to be excluded from low mobility zones (e.g. small pores), tend to remain within main flow paths with wider pore spaces and pore water velocities higher than the average groundwater velocity. Such movement through preferential flow paths explains that larger NPs (500 and 1000 nm) reach the outlet earlier than the tracer. This enhanced transport is consistent with observations described by Donath et al. (2019) and Shrestha and Kansakar (2016). In our experiments, it is observed in all replicas, being particularly pronounced for larger particles (1000 nm). Based on the R-values (Table 4) obtained from the modelling of NPs transport, the velocity increase in preferential flow can be calculated. Indeed, compared to the tracer, NP transport is enhanced by a factor of 1.06 for the 500 nm particles, and 1.22 for the 1000 nm particles. The size exclusion of MNPs is similar to that of colloids which show increases with colloid size, small porous media grain size, and low water content as observed by Bradford and Bettahar (2006).

According to modelling results, the effective diffusivity increases along with particle size (Table 4; Fig. 2A). Such a behaviour is linked to the rise of NP velocities with increasing size as a consequence of the size exclusion effect that boost transport of bigger plastic particles. The effective diffusivity includes dispersion that increases linearly with velocity. The effects of mean pore water velocity and particle size on dispersion were also observed by Chrysikopoulos and Katzourakis (2015).

While the variation over the replicas for D and K_d in Fig. 2 shows considerable deviations, the most significant dependency on particle size can be found for the removal rate (Fig. 2C). Losses represent particles that do not reach the outlet as they are trapped in smaller pores. The removal rate λ increases almost linearly by a factor of ten (from 1.87 x 10^{-6} to 17 x 10^{-6} s^{-1}) when the particle size increases by a factor of 8.33. This behaviour indicates that larger NPs entering small pore regions are much more likely to remain trapped.

3.4. Stability of particles and retention mechanisms

The hydrodynamic size and the zeta potential of the NPs from influent and effluent samples were measured to evaluate the particle stability and the interaction between NP-NP during the experiments (Table S3). These values were also used to applied DLVO theory assessing the interaction between NP-NP and the retention mechanisms of NPs in the sand matrix and AWI. The hydrodynamic particle size of NPs in the effluent presents small variations with respect to the values in the influent, indicating that homoaggregation between particles does not take place during infiltration through the sand. The zeta potential is negative for quartz sand (−33 mV) and NPs in the influent. This negative value remains relatively constant as particles infiltrate through the sand (Table S3) indicating their stability during transport. Despite a significant reduction of zeta potential value is observed for 120 nm NPs, shifting from −25.9 mV in the influent to −10.7 mV in the effluent, the high mass recovery and the absence of changes in particle size indicate that this parameter variation does not influence the transport dynamics of these NPs.

The DLVO interaction energy profiles between NP-NP, NP-Sand and NP-AWI under experimental conditions are shown in Fig. 3. The total interaction energy values demonstrate the dominance of electrostatic repulsion forces over van der Waals attraction forces, with a primary energy barrier formed at intermediate separation distances (20–30 nm) between NP particles. This suggests that the particles do not interact or aggregate, which is consistent with the stability findings described above. Similar results were obtained for NPs-sand interaction, suggesting an unfavourable environment for NPs to adhere to the sand grains, making increasingly challenging for them to overcome the energy barrier and to deposit onto sand surface. Comparing the DLVO energies, higher V_{TOT}^{max} values are obtained for 1000 nm (811.77 k_BT) with respect to 500 nm (329.25 k_BT) and 120 nm (53.65 k_BT), indicating a greater stability in the solution as the particle size increase. Similar trends have been observed for other nanoparticles in porous media (Pradel et al., 2020; Wang et al., 2022). While larger particles were expected to infiltrate through the sand due to their higher stability and higher repulsion from the surface, the recovered masses obtained in the experiments and the removal rate values from the modelling indicate the opposite. In the case of NP-AWI interaction, the lack of a negative primary and secondary energy minimums demonstrates that NPs were not retained in the AWI. This finding agrees with what has been observed by other authors in the literature. Chen et al. (2007), using column bubbles experiments, reported unfavourable conditions for the deposition of 220 nm NPs onto the AWI due to the strong repulsive electrostatic interactions. This behaviour was also observed by Bradford et al. (2002), Zhang et al. (2010), Mitropoulou et al. (2013) and Dong et al. (2022), among others. Chen et al. (2007) attributed the retention of the plastic particles to physical constraints at the small pore throats in the solid–water–air triple point developed under unsaturated conditions. This mechanism explains the increase of colloid retention with the decrease of water content (Dong et al., 2022; Fujita and Kobayashi, 2016; Liu et al., 2013). Moreover, since NPs do not penetrate the AWI, capillary

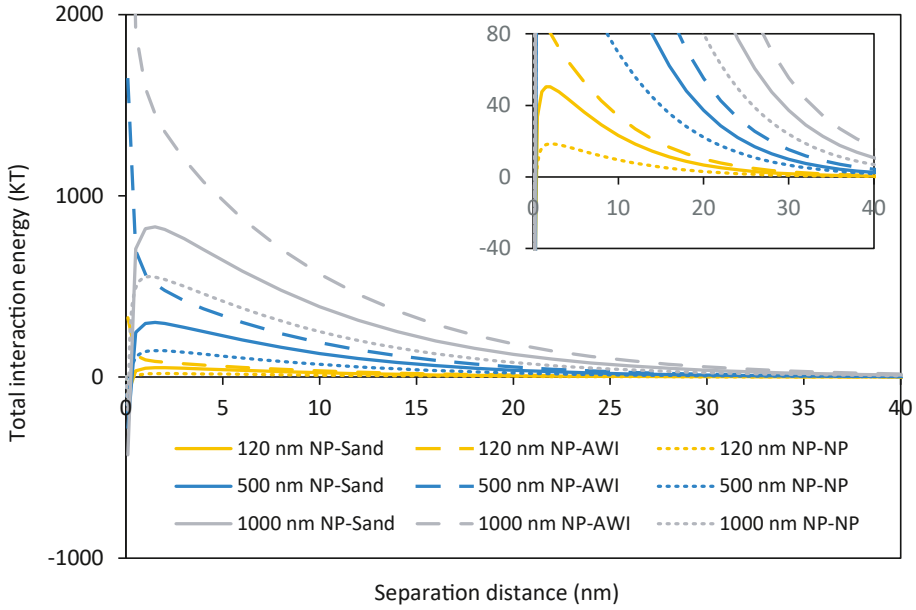

Fig. 3. Total interaction energy between 120, 500 and 1000 nm NP-NP particles (dotted line), NP-Sand (solid line) and NP-AWI (dashed line), as a function of the separation distance, according to the DLVO theory.

forces will not interact with these particles and hence will not influence on their retention within the porous media (Zhang et al., 2010; Aramrak et al., 2014).

Therefore, the retention of MNPs in the sand can be mainly attributed to physical retention mechanisms occurring at the pore scale. Bradford et al. (2002) describes the phenomenon of straining as a primary mechanism for the retention of colloidal particles, especially for larger particles that infiltrate through porous media with small pore sizes. When the ratio of the colloid particle size to the grain size (d_p/d_c) is greater than 0.0017, colloid trapping occurs in the pore throats of the sand, preventing their migration to deeper regions. In the present study, the ratio of MNP size to sand size is 0.002 for 1000 nm and 0.02 for 10, 000 nm, suggesting the occurrence of particle retention through straining phenomena. This mechanism has been also described for MNP retention by other authors. Dong et al. (2022) proved that the straining efficiency of 1200 nm polyethylene terephthalate (PET) MPs increases with decreasing grain size in unsaturated porous media due to the presence of small pores. Mitropoulou et al. (2013) attributed the retention of 2100 nm PSNP in unsaturated sand to straining. Other mechanisms, such as blocking and ripening, have been evoked to elucidate the retention of MNPs within porous media (Bradford and Torkzaban, 2008). Blocking occurs when the colloids deposited in available soil sites prevent the attachment of new colloids, leading to a decrease in the deposition rate. This process is represented by a rising plateau in the breakthrough curve during colloidal injection. Ripening is described as the adsorption of MNPs onto the soil surface followed by additional MNP adsorption onto those particles and manifests as a decline in the plateau over time (Mondal et al., 2021). The absence of such trends (and thus of associated processes) in the breakthrough curve of selected NPs underscores the dominance of straining at the small pore throats as the main mechanism of retention of MNPs.

3.4.1. Environmental implications

This study serves as an approach to understand the behaviour of MNPs in the environment and the mechanisms that affect their mobility in soils, and porous media in general, under unsaturated conditions. The results indicate that NPs exhibit a high infiltration capacity through porous media, enabling them to reach deeper horizons and potentially impact groundwater resources. NPs can act as vectors for other contaminants ("Trojan horse" effect), and they can additionally release plastic chemical additives that are not chemically bond to the polymer. Therefore, mobile NPs may disseminate through environmental compartments increasing the risk of contaminant release to deeper soil horizons and underlying water resources. On the contrary, larger particles suffer greater retention in porous media due to physical trapping in small-pore zones however, as highlighted by the modelling results, they also travel faster through the mean flow stream (size exclusion effect) approaching larger distance. Such outcomes highlight the role of soil structure as crucial for the transport of MNPs. At the same time, the reduction in the mobility of larger MNPs may also lead to their accumulation in the soil, potentially affecting its physico-chemical properties as well as becoming bioavailable for soil organisms and plant uptake processes. Therefore, this study provides useful information on the factors influencing the transport of MNPs under unsaturated conditions to, in turn, be helpful for better assessing the potential risks to ecosystems and, through them, to humans. Furthermore, the authors consider that this research encourages further investigation considering the physicochemical properties of natural soils.

4. Conclusions

This study explores the impact of particle size on the vertical transport of polystyrene MNPs through quartz sand under unsaturated conditions. The results show a significant correlation between MNP transport and particle size. Specifically, breakthrough curves and mass recovery values indicate that 120 nm particles are highly mobile (95.11 ± 2.93%) compared to 500 nm (85.73 ± 2.07%) and 1000 nm (71.44 ± 3.30%). Whereas 10,000 nm MP display the lowest mobility since they are fully retained in the porous media. The NP transport model reveals that larger particles (1000 nm) are more susceptible to being immobilized in small-porosity zones than smaller ones due to physical retention processes, resulting in higher removal rates and lower retrieval. When not immobilized, larger MNP particles travel at higher velocities along preferential flow paths due to the size exclusion effect, resulting in shorter arrival times at the column outlet compared to the tracer. Indeed, travel times decrease by factors of 0.94 and 0.82 for 500 and 1000 nm, respectively. Minimal variations observed in both hydrodynamic particle size and zeta potential of NPs in the effluent samples suggest the lack of particle homoaggregation. According to the DLVO theory, NP-NP interaction and NP aggregation onto the quartz matrix or

air-water interface is unlikely to occur due to the dominance of electrostatic repulsion forces over the van der Waals forces and the absence of negative primary and secondary energy minimums. Hence, the retention of MNP can be primary attributed to physical processes of straining in small pore throats between sand grains and at the solid–water–air triple point. Our findings contribute to the knowledge on the dynamics and processes developed during the migration of MNPs through porous media under unsaturated conditions, underscoring the crucial role of enhanced transport in their fate, like colloids. The better understanding of MNP behaviour and exposure is essential to evaluate the potential risks posed by these contaminants to human health and ecosystems.

CRediT authorship contribution statement

Cynthia Rieckhof: Writing – review & editing, Writing – original draft, Visualization, Methodology, Investigation, Formal analysis. **Virtudes Martínez-Hernández:** Writing – review & editing, Supervision, Methodology, Conceptualization. **Ekkehard Holzbecher:** Writing – review & editing, Writing – original draft, Software, Formal analysis. **Raffaella Meffe:** Writing – review & editing, Supervision, Methodology, Conceptualization.

Declaration of competing interest

The authors declare that they have no known competing financial interests or personal relationships that could have appeared to influence the work reported in this paper.

Acknowledgments

This study has received funding from the project PAPILLONS funded under European Union's Horizon 2020 research and innovation programme (grant agreement No 101000210) and from μNanoCare, grant RTC2019-007261-5 funded by MICIU/AEI/10.13039/501100011033. The authors thank Leonor Nozal and Raúl Alonso del Águila from the University of Alcalá for providing the experimental data that allowed the assessment of the stability of nanoplastic particles.

Appendix A. Supplementary data

Supplementary data to this article can be found online at https://doi.org/10.1016/j.envpol.2024.125193.

Data availability

Data will be made available on request.

References

Aramrak, S., Flury, M., Harsh, J.B., Zollars, R.L., 2014. Colloid mobilization and transport during capillary fringe fluctuations. Environ. Sci. Technol. 48 (13), 7272–7279. https://doi.org/10.1021/es501797y.

Babakhani, P., 2019. The impact of nanoparticle aggregation on their size exclusion during transport in porous media: one- and three-dimensional modelling investigations. Sci. Rep. 9 (1), 14071. https://doi.org/10.1038/s41598-019-50493-6.

Bradford, S.A., Yates, S.R., Bettahar, M., Simunek, J., 2002. Physical factors affecting the transport and fate of colloids in saturated porous media. Water Resour. Res. 38 (12). https://doi.org/10.1029/2002wr001340, 63-1.

Bradford, S.A., Simunek, J., Bettahar, M., Van Genuchten, M.T., Yates, S.R., 2003. Modeling colloid attachment, straining, and exclusion in saturated porous media. Environ. Sci. Technol. 37, 2242–2250. https://doi.org/10.1021/es025899u.

Bradford, S.A., Bettahar, M., 2006. Concentration dependent transport of colloids in saturated porous media. J. Contam. Hydrol. 82, 99–117. https://doi.org/10.1016/j.jconhyd.2005.09.006.

Bradford, S.A., Torkzaban, S., 2008. Colloid transport and retention in unsaturated porous media: a review of interface-, collector-, and pore-scale processes and models. Vadose Zone J. 7, 667–681. https://doi.org/10.2136/vzj2007.0092.

Bradford, S.A., Torkzaban, S., 2015. Determining parameters and mechanisms of colloid retention and release in porous media. Langmuir 31 (44), 12096–12105. https://doi.org/10.1021/acs.langmuir.5b03080.

Chen, G., Abichou, T., Tawfiq, K., Subramaniam, P.K., 2007. Impact of surface charge density on colloid deposition in unsaturated porous media. Colloids Surf A: Physicochem. Eng. Asp. 302 (1–3), 342–348. https://doi.org/10.1016/j.colsurfa.2007.02.063.

Chrysikopoulos, C.V., Syngouna, V.I., 2014. Effect of gravity on colloid transport through water-saturated columns packed with glass beads: modeling and experiments. Environ. Sci. Technol. 48 (12), 6805–6813. https://doi.org/10.1021/es501295n.

Chrysikopoulos, C.V., Katzourakis, V.E., 2015. Colloid particle size-dependent dispersivity. Water Resour. Res. 51 (6), 4668–4683. https://doi.org/10.1002/2014WR016094.

COMSOL, 2019. COMSOL Multiphysics Reference Manual Version, 5.5. COMSOL.

De Smedt, F., Wierenga, P.J., 1984. Solute transfer through columns of glass beads. Water Resour. Res. 20 (2), 225–232. https://doi.org/10.1029/WR020i002p00225.

Derjaguin, B., Landau, L., 1993. Theory of the stability of strongly charged lyophobic sols and of the adhesion of strongly charged particles in solutions of electrolytes. Prog. Surf. Sci. 43 (1–4), 30–59. https://doi.org/10.1016/0079-6816(93)90013-L.

Donath, A., Kantzas, A., Bryant, S., 2019. Opportunities for particles and particle suspensions to experience enhanced transport in porous media: a review. Transport Porous Media 128, 459–509. https://doi.org/10.1007/s11242-019-01256-4.

Dong, Z., Qiu, Y., Zhang, W., Yang, Z., Wei, L., 2018. Size-dependent transport and retention of micron-sized plastic spheres in natural sand saturated with seawater. Water Res. 143, 518–526. https://doi.org/10.1016/j.watres.2018.07.007.

Dong, S., Zhou, M., Su, X., Xia, J., Wang, L., Wu, H., Suakollie, E.B., Wang, D., 2022. Transport and retention patterns of fragmental microplastics in saturated and unsaturated porous media: a real-time pore-scale visualization. Water Res. 214. https://doi.org/10.1016/j.watres.2022.118195.

Elimelech, M., Gregory, J., Jia, X., Williams, R.A., 1995. Particle Deposition and Aggregation: Measurement, Modelling and Simulation. Butterworth-Heinemann, Oxford. https://doi.org/10.1016/B978-0-7506-7024-1.X5000-6.

Flury, M., Qiu, H., 2008. Modeling colloid-facilitated contaminant transport in the vadose zone. Vadose Zone J. 7 (2), 682–697. https://doi.org/10.2136/vzj2007.0066.

Fujita, Y., Kobayashi, M., 2016. Transport of colloidal silica in unsaturated sand: effect of charging properties of sand and silica particles. Chemosphere 154, 179–186. https://doi.org/10.1016/j.chemosphere.2016.03.105.

Gao, J., Pan, S., Li, P., Wang, L., Hou, R., Wu, W.M., Luo, J., Hou, D., 2021. Vertical migration of microplastics in porous media: multiple controlling factors under wet-dry cycling. J. Hazard Mater. 419, 126413. https://doi.org/10.1016/j.jhazmat.2021.126413.

Gregory, J., 1975. Interaction of unequal double layers at constant charge. J. Colloid Interface Sci. 51, 44–51. https://doi.org/10.1016/0021-9797(75)90081-8.

Gregory, J., 1981. Approximate expressions for retarded van der waals interaction. J. Colloid Interface Sci. 83, 138–145. https://doi.org/10.1016/0021-9797(81)90018-7.

He, Y.T., Wan, J., Tokunaga, T., 2008. Kinetic stability of hematite nanoparticles: the effect of particle sizes. J. Nanopart. Res. 10, 321–332. https://doi.org/10.1007/s11051-007-9255-1.

Hidalgo-Ruz, V., Gutow, L., Thompson, R.C., Thiel, M., 2012. Microplastics in the marine environment: a review of the methods used for identification and quantification. Environ. Sci. Technol. 46 (6), 3060–3075. https://doi.org/10.1021/es2031505.

Hotze, E.M., Phenrat, T., Lowry, G.V., 2010. Nanoparticle aggregation: challenges to understanding transport and reactivity in the environment. J. Environ. Qual. 39 (6), 1909–1924. https://doi.org/10.2134/jeq2009.0462.

Hou, Y., Luo, C., Wang, Y., Zhao, Y., Qiu, Y., 2022. Nanoplastics dominate the cotransport of small-scale plastics in seawater-saturated porous media. Water Res. 221, 118773. https://doi.org/10.1016/j.watres.2022.118773.

Huang, K., Toride, N., Van Genuchten, M.T., 1995. Experimental investigation of solute transport in large, homogeneous and heterogeneous, saturated soil columns. Transport Porous Media 18, 283–302. https://doi.org/10.1007/BF00616936.

Hurley, R.R., Nizzetto, L., 2018. Fate and occurrence of micro(nano)plastics in soils: knowledge gaps and possible risks. Curr. Opin. Environ. Sci. Health 1, 6–11. https://doi.org/10.1016/j.coesh.2017.10.006.

Israelachvili, J.N., 1992. Interfacial forces. J. Vac. Sci. Technol. 10 (5), 2961–2971. https://doi.org/10.1116/1.577894.

Jin, Y., Yates, M.V., Thompson, S.S., Jury, W.A., 1997. Sorption of viruses during flow through saturated sand columns. Environ. Sci. Technol. 31 (2), 548–555. https://doi.org/10.1021/es9604323.

Kedzierski, M., Cirederf-Boulant, D., Palazot, M., Yvin, M., Bruzaud, S., 2023. Continents of plastics: an estimate of the stock of microplastics in agricultural soils. Sci. Total Environ. 880. https://doi.org/10.1016/j.scitotenv.2023.163294.

Keller, A.S., Jimenez-Martinez, J., Mitrano, D.M., 2020. Transport of nano- and microplastic through unsaturated porous media from sewage sludge application. Environ. Sci. Technol. 54, 911–920. https://doi.org/10.1021/acs.est.9b06483.

Kutralam-Muniasamy, G., Shruti, V.C., Pérez-Guevara, F., Roy, P.D., 2023. Microplastic diagnostics in humans: "The 3Ps" Progress, problems, and prospects. Sci. Total Environ. 856, 159164. https://doi.org/10.1016/j.scitotenv.2022.159164.

Li, W., Brunetti, G., Zafiu, C., Kunaschk, M., Debreczeby, M., Stumpp, C., 2024. Experimental and simulated microplastics transport in saturated natural sediments: impact of grain size and particle size. J. Hazard Mater. 468, 133772. https://doi.org/10.1016/j.jhazmat.2024.133772.

Lin, D., Hu, L., Bradford, S.A., Zhang, X., Lo, I.M.C., 2021. Pore-network modeling of colloid transport and retention considering surface deposition, hydrodynamic

bridging, and straining. J. Hydrol. (Amst) 603, 127020. https://doi.org/10.1016/j.jhydrol.2021.127020.
Liu, L., Gao, B., Wu, L., Morales, V.L., Yang, L., Zhou, Z., Wang, H., 2013. Deposition and transport of graphene oxide in saturated and unsaturated porous media. Chem. Eng. J. 229, 444–449. https://doi.org/10.1016/j.cej.2013.06.030.
Lloyd, J.W., Heathcote, J.A., 1985. Natural Inorganic Hydrochemistry in Relation to Ground Water, an Introduction. Clarendon Press, Oxford. New York.
Mitropoulou, P.N., Syngouna, V.I., Chrysikopoulos, C.V., 2013. Transport of colloids in unsaturated packed columns: role of ionic strength and sand grain size. Chem. Eng. J. 232, 237–248. https://doi.org/10.1016/j.cej.2013.07.093.
Mondal, A., Dubey, B.K., Arora, M., Mumford, K., 2021. Porous media transport of iron nanoparticles for site remediation application: a review of lab scale column study, transport modelling and field-scale application. J. Hazard Mater. 403, 123443. https://doi.org/10.1016/j.jhazmat.2020.123443.
Nutzmann, G., Maciejewski, S., Joswig, K., 2002. Estimation of water saturation dependence of dispersion in unsaturated porous media: experiments and modelling analysis. Adv. Water Res. 25 (5), 565–576. https://doi.org/10.1016/S0309-1708(02)00018-0.
Pradel, A., Hadri, H. el, Desmet, C., Ponti, J., Reynaud, S., Grassl, B., Gigault, J., 2020. Deposition of environmentally relevant nanoplastic models in sand during transport experiments. Chemosphere 255, 126912. https://doi.org/10.1016/j.chemosphere.2020.126912.
Rajan, M., Karunanidhi, D., Jaya, J., Preethi, B., Subramani, T., Aravinthasamy, P., 2024. A comprehensive review on human health hazards due to groundwater contamination: a global perspective. Phys. Chem. Earth, Parts A/B/C 135, 103637. https://doi.org/10.1016/j.pce.2024.103637.
Shaniv, D., Dror, I., Berkowitz, B., 2021. Effects of particle size and surface chemistry on plastic nanoparticle transport in saturated natural porous media. Chemosphere 262, 127854. https://doi.org/10.1016/j.chemosphere.2020.127854.
Shrestha, I.N., Kansakar, P., 2016. Comparison Of Preferential Flow Of Solute In Porous Media With Darcy's Flow. International Journal of Scientific & Technology Research 5, 7.
Sim, Y., Chrysikopoulos, C.V., 1995. Analytical models for one-dimensional virus transport in saturated porous media. Water Resour. Res. 31, 1429–1437. https://doi.org/10.1029/95WR00199.
Song, Z., Yang, X., Chen, F., Zhao, F., Zhao, Y., Ruan, L., Wang, Y., Yang, Y., 2019. Fate and transport of nanoplastics in complex natural aquifer media: effect of particle size and surface functionalization. Sci. Total Environ. 669, 120–128. https://doi.org/10.1016/j.scitotenv.2019.03.102.
Verwey, E.J.W., 1947. Theory of the stability of lyophobic colloids. J. Phys. Colloid Chem. 51, 631–636. https://doi.org/10.1021/j150453a001.
Wang, Y., Xu, L., Chen, H., Zhang, M., 2022. Retention and transport behavior of microplastic particles in water-saturated porous media. Sci. Total Environ. 808, 152154. https://doi.org/10.1016/j.scitotenv.2021.152154.
Winiarska, E., Jutel, M., Zemelka-Wiacek, M., 2024. The potential impact of nano- and microplastics on human health: understanding human health risks. Environ. Res. 251, 118535. https://doi.org/10.1016/j.envres.2024.118535.
Wu, X., Zeng, X., Lyu, X., Gao, B., Sun, Y., Wu, J., 2022. Combined effects of Fe/Al oxyhydroxide coating and pH on polystyrene nanoplastic transport in saturated sand media. Water Air Soil Pollut. 233 (1), 2. https://doi.org/10.1007/s11270-021-05469-6.
Xi, X., Wang, L., Zhou, T., Yin, J., Sun, H., Yin, X., Wang, N., 2022. Effects of physicochemical factors on the transport of aged polystyrene nanoparticles in saturated porous media. Chemosphere 289, 133239. https://doi.org/10.1016/j.chemosphere.2021.133239.
Yasir, A.M., Ma, J., Ouyang, X., Zhao, J., Zhao, Y., Weng, L., Islam, M.S., Chen, Y., Li, Y., 2022. Effects of selected functional groups on nanoplastics transport in saturated media under diethylhexyl phthalate co-contamination conditions. Chemosphere 286, 131965. https://doi.org/10.1016/j.chemosphere.2021.131965.
You, Z., Badalyan, A., Bedrikovetsky, P., 2013. Size-exclusion colloidal transport in porous media—stochastic modeling and experimental study. SPE J. 18, 620–633. https://doi.org/10.2118/162941-PA.
Yu, Y., Flury, M., 2021. Current understanding of subsurface transport of micro- and nanoplastics in soil. Vadose Zone J. 20 (2), 20108. https://doi.org/10.1002/vzj2.20108.
Zhang, W., Morales, V.L., Cakmak, M.E., Salvucci, A.E., Geohring, L.D., Hay, A.G., Parlange, J.Y., Steenhuis, T.S., 2010. Colloid transport and retention in unsaturated porous media: effect of colloid input concentration. Environ. Sci. Technol. 44 (13), 4965–4972. https://doi.org/10.1021/es100272f, 2010.
Zhang, Y., Hartung, M.B., Hawkins, A.J., Dekas, A.E., Li, K., Horne, R.N., 2021. DNA tracer transport through porous media—the effect of DNA length and adsorption. Water Resour. Res. 57 (2). https://doi.org/10.1029/2020WR028382.
Zhang, H., Cheng, H., Wang, Y., Duan, Z., Cui, W., Shi, Y., Qin, L., 2022. Influence of functional group modification on the toxicity of nanoplastics. Front. Mar. Sci. 8, 800782. https://doi.org/10.3389/fmars.2021.800782.
Zhao, W., Zhao, Y., Geng, T., Tian, Y., Zhao, P., 2023. Co-transport behavior and Trojan-horse effect of colloidal microplastics with different functional groups and heavy metals in porous media. J. Hazard Mater. 459, 131892. https://doi.org/10.1016/j.jhazmat.2023.131892.
Zhou, D., Cai, Y., Yang, Z., 2022. Key factors controlling transport of micro- and nanoplastic in porous media and its effect on coexisting pollutants. Environ. Pollut. 293, 118503. https://doi.org/10.1016/j.envpol.2021.118503.